

Hot-electron bolometric mixer with negative differential resistance

Chang Yoo^{1,3}, Akim A. Babenko^{1,2}, and Boris S. Karasik^{1,a)}

Abstract — We demonstrate that the conversion gain of a superconducting hot-electron bolometer (HEB) mixer can be increased by biasing the device within the negative differential resistance (NDR) region of its current–voltage characteristic. Although NDR biasing has historically been avoided due to MHz-range resistive oscillations, we show that these oscillations arise from an LC resonance formed by the bias-T inductance and the effective thermal capacitance of the HEB. By applying stability criteria analogous to those developed for tunnel diodes, we redesigned the embedding circuit to suppress this resonance and achieve stable NDR operation. Direct measurements using two monochromatic 2.5-THz sources confirm the predicted gain enhancement. These results establish NDR biasing as a viable method for improving HEB mixer performance and motivate further studies of noise behavior and circuit optimization.

Affiliations:

¹ Jet Propulsion Laboratory, California Institute of Technology, Pasadena, CA 91109, USA

² Currently, with Google Quantum AI, Goleta, CA 93111, USA

³ Currently, with xLight, Palo Alto, CA 94306, USA

a) **Author to whom correspondence should be addressed:**

boris.s.karasik@jpl.nasa.gov

Superconducting resistive bolometers are essential for remote sensing, spectroscopy, and quantum information applications. Although they require cryogenic cooling, they outperform non-superconducting sensors in many high-sensitivity regimes. Depending on the readout method, these devices operate either as direct detectors—transition-edge sensors (TES)—or as heterodyne mixers, known as hot-electron bolometers (HEBs). TES devices, typically fabricated from low- T_c materials such as Ti, W, Al, Mo, and their bilayers with Au or Cu, use these materials as thermometers. Their heat capacity and thermal conductance to the heat sink are controlled by mechanical design, often employing Si_xN_y membranes. This approach allows independent tuning of TES parameters, enabling low thermal conductance G for high responsivity and reduced heat capacity C for millisecond-scale thermal time constants $\tau_{th} = C/G$ ¹.

Another TES approach uses the hot-electron effect, where thermal conductance is dominated by weak electron-phonon coupling ². In thin films configuration, thermal phonons escape without returning energy to the electrons, so the effective thermal conductance is set by electron-phonon interactions, and the thermal time constant corresponds to the intrinsic electron-phonon scattering time $\tau_{th} = \tau_{e-ph}$.

HEB mixers ^{3,4}, which are critical for astrophysics in the 1.3-6 THz range, operate on similar principles, but in practical HEB devices the phonon escape time is non-negligible, leading in combination with τ_{e-ph} to thermal time constants of several tens of picosecond. This is necessary to achieve intermediate frequency (IF) bandwidth of several GHz. As a result, only NbN films with a thickness of 3–5 nm and MgB_2 films of 5–10 nm have demonstrated successful HEB mixer performance.

TES performance improves under voltage bias due to negative electro-thermal feedback (n-ETF), which stabilizes the bias point. Optimal operation occurs in the negative differential resistance (NDR) region, where the device exhibits a faster response, higher responsivity, and reduced Johnson and readout noise ⁵. Most TES devices remain stable because the electrical time constant $\tau_{el} = L_{SQUID}/(R + R_B) \sim 0.1\text{--}1 \mu\text{s}$ is much smaller than the thermal time constant $\tau_{th} \sim \text{ms}$ (L_{SQUID} is the SQUID readout input coil, $R_B \leq 1 \text{ Ohm}$ is the bias resistor, R is the TES ohmic resistance). Analyses ^{6,7} confirms these conditions satisfy stability requirements.

In principle, n-ETF could similarly enhance HEB mixer performance by increasing conversion gain⁸ and reducing the system noise temperature. However, this approach has not yet been used in HEB mixers due to the short thermal time constant $\tau_{th} \sim$ tens of picosecond along the more complex external electrical embedding circuit. In a superconducting HEBs, the NDR regime can be reached by lowering the local oscillator (LO) power, which produces an N-shaped current-voltage characteristic (IVC). However, operating in this regime often triggers MHz-range oscillations that prevent stable mixer operation⁹⁻¹⁴. These oscillations have been attributed to magnetic vortex motion¹⁰⁻¹², but circuit analysis shows that NDR amplifies resonances caused by reactive components in the bias network. In such cases, the oscillation frequency is set by the LC resonance rather than vortex dynamics.

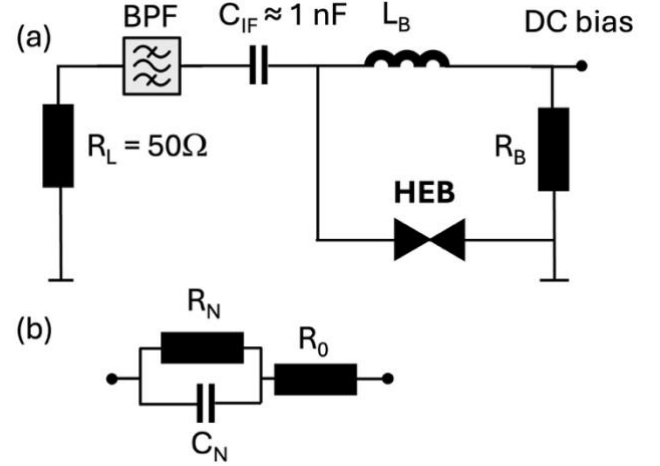


Figure 1. (a) Schematic of a typical HEB bias/IF circuit. In our experiment, $R_B = 15$ Ohm, $L_B = 2$ μ H or 220 nH, or 70 nH. The resulting equivalent bandpass filter (BPF) bandwidth was 0.8-2 GHz. (b) Equivalent electrical circuit of the HEB mixer. The component values correspond to the parameters of the bolometer (see Table I).

Well-known examples of passive solid-state NDR devices include tunnel diodes and Gunn diodes. Methods for stabilizing the bias point in resonant tunneling diodes (RTDs) have been studied since the 1960s, and the resulting criteria apply broadly to any NDR device.¹⁵⁻²⁰

The objective of the current work was to resolve the instability issue in HEB mixer devices with NDR and demonstrate the mixer operation with an increase in conversion gain. We consider the typical

TABLE I. Relationship between the electrical model and bolometric physical parameters.

Equivalent circuit parameter	Relation to the bolometric parameters
R_0	$R (\equiv V/I)$
R_N	$2LR/(1 - \mathcal{L}) (< 0 \text{ for NDR})$
$Z(0) \equiv dV/dI = R_0 + R_N$	$R(1 + \mathcal{L})/(1 - \mathcal{L}) (< 0 \text{ for NDR})$
C_N	$\tau_{th}/(2R\mathcal{L})$

HEB bias/IF circuit including the bias-T inductance L_B , the IF coupling capacitor C_{IF} , and the DC bias resistor R_B . The IF line includes an L-band isolator and a low-noise amplifier (LNA) modeled as a 50-Ohm termination (Fig. 1(a)). Because the IF bandwidth (0.8–2 GHz) is far above the parasitic oscillation frequencies, it is excluded from the stability analysis.

The HEB device is modeled as two resistors (R_0 and R_N) in series, with R_N being shunted by a capacitor C_N (Fig. 1(b)) This representation follows the bolometric impedance model for the HEB ^{8,21,22} and has been experimentally validated ^{8,23-25}. The resistor R_N represents the inertial part of the differential resistance that vanishes at frequencies above the thermal response speed τ_{th}^{-1} . The resistor R_0 is a real part of the bolometer impedance that remains constant over a broad frequency range $\tau_{th}^{-1} < \omega < 2\Delta/\hbar$ where Δ is the maximum superconducting gap in the resistive state. In most cases, $R_0 = R = V/I$ ^{8,25}, although a moderate current dependence $R(I)$ has been observed in the vortex-driven resistive ²³ state. In the following, we assume $R_0 = R$. The capacitance C_N represents the equivalent of the thermal inertia.

The IF impedance of the HEB is given by the lumped-element bolometric theory ^{21,23}:

$$Z(\omega) = R \frac{1+\mathcal{L}}{1-\mathcal{L}} \cdot \frac{1+j\omega\tau_{th}/(1+\mathcal{L})}{1+j\omega\tau_{th}/(1-\mathcal{L})}. \quad (1)$$

Here \mathcal{L} is the dimensionless parameter called the “self-heating parameter” in the HEB community and “the electro-thermal feedback loop gain” in the TES community. We use the standard TES notation to distinguish it from other notations in this paper. $\mathcal{L} \equiv dP_J/(GdT_e)$ is always positive and depends on the shape of the IVC (P_J is the Joule power dissipated at the bias point). For the NDR case where $Z(0) < 0$, $\mathcal{L} > 1$.

The equivalent circuit of Fig. 1(b) ⁸ yields:

$$Z(\omega) = R_0 + \frac{R_N}{1+j\omega R_N C_N}. \quad (2)$$

Comparison of Eqs. (1) and (2) yields the relationships summarized in Table I.

We initially used a commercial bias-T with an inductance $L_B \approx 2 \mu\text{H}$ (room temperature value) and a coupling capacitor $C_{IF} = 1 \text{ nF}$. With this circuit, we carried out experiments using a common quasioptical HEB mixer design, where the mixer device integrated with a log-spiral antenna on a silicon chip is placed on a

hyperhemispherical Si lens for coupling to THz radiation. The device parameters are listed in Table II. A 2.52-THz methanol gas laser served as local oscillator (LO), and a weak signal from a frequency multiplier chain (FMC) offset by 1.4 GHz was injected into the mixer through the same port as the LO to monitor the intermediate frequency (IF) output at 1.4 GHz, which was proportional to the mixer conversion gain.

With this circuit, the NDR region was unstable. Figure 2 (blue symbols) shows a plateau with a kink instead of a smooth NDR region. Instead of a single 1.4 GHz peak, the IF spectrogram (inset in Fig. 2) exhibited intermodulation sidebands spaced by 10-20 MHz depending on the position of the bias point, consistent with the expected LC resonance frequency $f_{osc} \approx 1/(2\pi\sqrt{L_B C_N}) \sim \text{few } 10\text{s MHz}$ ($C_N \sim \text{a few ps}$). Large-amplitude switching between two IVC points also occurred, producing time-averaged distortions in the measured IVC. This effect was reported in many HEB papers (see, e.g., ^{26,27}) but has never been properly explained. However, an identical behavior of the unstable IVC with NDR was studied and explained for tunnel diodes ^{28,29}. Another evidence of the spurious nature of the IVC with NDR is the

TABLE II. Characteristics of the HEB device

Parameter	Value
Film thickness	5-6 nm
Substrate	Si with MgO buffer
Normal resistance	103 Ohm
Critical temperature	11.1 K
Superconducting transition width	2.5 K
Critical current at 4.2 K	240 μA

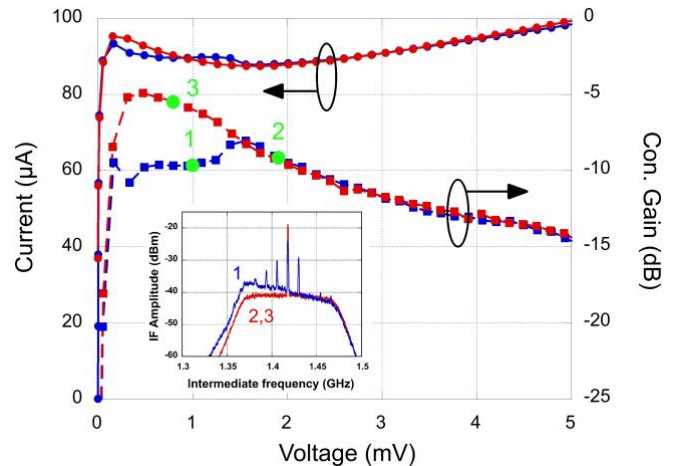


Figure 2. IVCs and corresponding conversion-gain curves vs bias. Blue symbols correspond to $L_B = 2 \mu\text{H}$ and red symbols are for $L_B = 220 \text{ nH}$. The plateau on the “blue” IVC below 1.5 mV is the result of time-average oscillations caused by the instability of the bias point. The conversion gain values in this region are also uncertain and deviate from the steady trend above 1.5 mV. The inset shows the intermodulated components (10-20 MHz) caused by the bias point oscillation around the mixing tone at $\approx 1.4 \text{ GHz}$ (point 1). In the steady states (points 2 and 3), these components are absent.

conversion gain behavior. When the bias is swept along the stable IVC (see Fig. 2) the gain changes smoothly and monotonically. However, in the NDR range the gain drops dramatically. This because there is no real stationary IVC and the observed gain values are just time averaged random samples captured by the spectrum analyzer.

The HEB circuit resembles the circuit used to analyze the Esaki tunnel diode closely. The stability of tunnel diodes with NDR was studied intensively by solving the circuit differential equations and identifying the solution leading to damped or overdamped oscillations¹⁹. In the terms used in this paper, the general criteria can be summarized into two conditions¹⁷:

$$R_{DC} < |Z(0)|, Z(0) = dV/dI \quad (3a)$$

$$\omega_r < \omega_x \quad (3b)$$

Here $R_{DC} = R_0 + R_B$ is the total resistance in series with the pure negative R_N . $\omega_r = (R_N C_N)^{-1} \sqrt{R_N/R_S - 1}$ is the frequency point where the real part of the total circuit impedance turns zero, $\text{Re}[Z_{tot}(\omega_r)] = 0$. Similarly, $\omega_x = \sqrt{(L_b C_N)^{-1} - (R_N C_N)^{-2}}$ yields $\text{Im}[Z_{tot}(\omega_x)] = 0$. Equation (3a) states that the load line's DC resistance, R_{DC} , must be less than the absolute value of the NDR, $|Z(0)|$; that is, the load line intersects the IVC at only one point (so-called "voltage bias", in TES terminology). This prevents the device from switching between points on the IVC where $Z(0) > 0$ and the bias is stable, across the NDR bias range where $Z(0) < 0$. Equation (3b) states that the characteristic frequency of the resonance should be away from the range where $\text{Re}(Z) < 0$ so the oscillations are damped.

Using Table I, condition 3(b) can be reduced to the following:

$$L_B < \tau_{th}(R_B + R)/(\mathcal{L} - 1). \quad (4)$$

Although the lumped-element model describes NbN HEB only qualitatively due to their hot-spot nature^{30,31}, ((4) provides useful guidance: L_B must be minimized, and R_B should be as large as possible while still satisfying Eq. (3a).

Following Eq. (4), we replaced the commercial bias-T with a custom-made one, using high-frequency PiconicsTM air-core inductors $L_B = 220$ nH or 70 nH. The bias resistance remained unchanged ($R_B = 15$

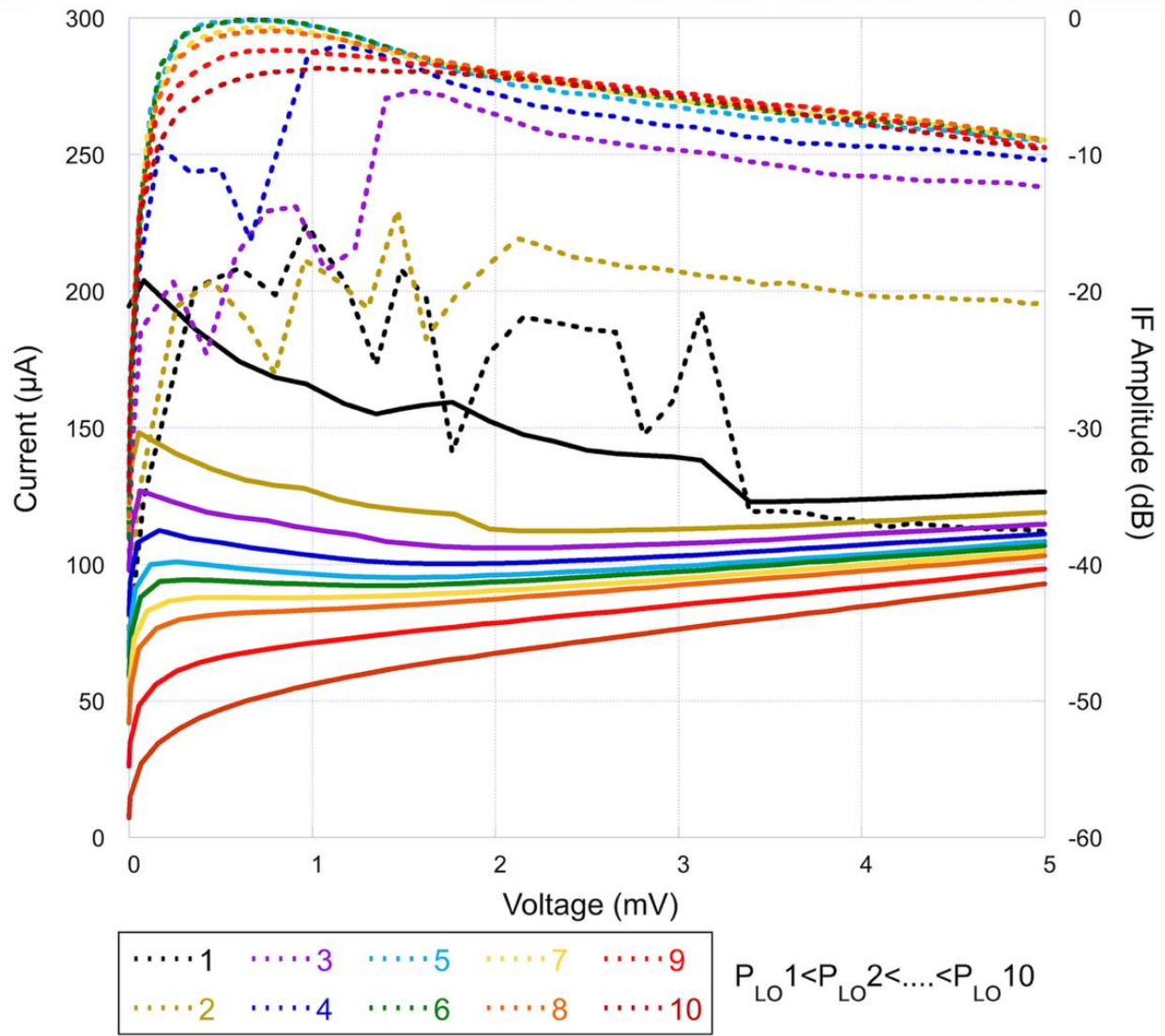


Figure 3. Gradual transition from NDR to PDR as the LO power decreases (curves numbers from 1 to 10), and $L_B = 70$ nH. Solid lines are IVCs, dashed lines are IF output power (proportional to the conversion gain). Same line colors correspond to the same P_{LO} values. Gain curves 5 and 6 are almost indistinguishable.

Ohm). This made the IVC continuous (Fig.2, red symbols), and the IF spectrum reduced to a single tone. Further reduction of the LO power (smaller $|Z(0)|$ and larger \mathcal{L} values) led again to instabilities but the frequency of the intermodulation sidebands became of the order of 100 MHz, roughly corresponding to a lower L_B value.

Figure 3 shows the gradual transition of the PDR into NDR when the LO power is decreased in small steps and $L_B = 70$ nH. The behavior of the conversion gain is similar to that in Fig. 2: for the IVCs with low pumping level, the NDR regions exhibited kinks, and the apparent conversion gain was low and choppy, as the bias was swept. Starting from curve 5, the NDR bias was stable. The highest gain was

achieved for curves 5 or 6 (almost no difference), maybe slightly higher than in the case of $L_B = 220$ nH, since the critical current (and \mathcal{L} value) was higher.

The gain in the NDR regime is a few dB higher than in the PDR regime (Fig. 3). The moderate magnitude of this effect is mostly due to the mixer bandwidth compression for \mathcal{L} values only slightly greater than 1 that was possible to achieve in this experimental work. At least qualitatively, the gain and the mixer time

can be explained by the lumped-element model equations:

$$\eta = 2\mathcal{L}^2(P_{LO}/P_J) \frac{RR_L}{(R+R_L)^2} \frac{1}{\left(1+\mathcal{L}\frac{R-R_L}{R+R_L}\right)^2} \frac{1}{1+(\omega_{IF}\tau^*)^2} \quad (5a)$$

$$\tau^* = \tau_{th} / \left(1 + \mathcal{L} \frac{R-R_L}{R+R_L}\right) \quad (5b)$$

Here $\omega_{IF} = 2\pi \times 1.4$ GHz and $\tau_{th} \approx 60$ ps for our 5-6 nm thick film^{32,33}, $R_L = 50$ Ohm is the IF line impedance. In our case, $R \approx 5$ Ohm (the peak gain value in Figs. 2 and 3), the maximum \mathcal{L} value is ≈ 1.1 as estimated from the experiment IVC and Eq. (1) assuming $\omega_{IF} = 0$. Then $\tau^* \approx 10 \times \tau_{th}$ and the overall gain η is a factor of ≈ 14 -15 dB lower than it would have been for $\omega_{IF} \approx 0$. For HEB mixers with shorter τ_{th} , the NDR effect on the gain at 1.4 GHz would be more significant.

Further gain improvement requires larger values \mathcal{L} , which demands smaller values of $|Z(0)|$. Equation (4) indicates that this requires even smaller L_B . For the inductive bias-T, the limit is set by potential leakage of the IF power into the bias circuit. With $L_B = 220$ nH, the inductive impedance at 1.4 GHz is $X_L \approx 1.93$ kOhm, which is substantially larger than the 50-Ohm input impedance of the LNA. For $L_B = 70$ nH, $X_L \approx 625$ Ohm, which is still more than an order of magnitude greater than 50 Ohm. For smaller L_B , X_L would become comparable to 50 Ohm. So, 70 nH is probably nearly the limit to which the bias-T inductance can be pushed for the given IF.

An additional pathway for increasing the gain in the current HEB device is the optimization of the DC-bias resistor R_B , which was not addressed in this work. According to Eq. (4), increasing R_B allows for a larger value of \mathcal{L} ; however, the limiting condition from Eq. (3a) must still be satisfied. Substantial

experimental effort will be required to determine the optimal combination of R_B and L_B that maximizes both \mathcal{L} and the conversion gain.

Finally, a more radical approach to mitigating parasitic oscillations is to eliminate the bias inductor L_B altogether. In this inductorless configuration, bias resistor R_B appears in parallel with the HEB and R_L , partially shunting the IF signal (Fig. 4). This introduces a multiplication factor of $R_B/(R_L + R_B)$ in Eq. (5a). Besides, the IF impedance presented to the HEB is not R_L only but the parallel connection of R_L and R_B , $R_L^* = R_L R_B / (R_L + R_B)$. Hence, the system of Eqs. (5) then becomes:

$$\eta_{no_L} = 2\mathcal{L}^2 (P_{LO}/P_J) \frac{RR_L^*}{(R+R_L^*)^2} \frac{1}{\left(1 + \mathcal{L} \frac{R-R_L^*}{R+R_L^*}\right)^2} \frac{R_B}{R_L+R_B} \frac{1}{1+(\omega_{IF}\tau^*)^2} \quad (6a)$$

$$\tau^* = \tau_{th} / \left(1 + \mathcal{L} \frac{R-R_L^*}{R+R_L^*}\right) \quad (6b)$$

We compare the η_{no_L} value, assuming $\mathcal{L} = 2$ and $R = 5$ Ohm with the unshunted η value in the PDR regime (Eq. (5a)), where the self-heating parameter is at its highest possible (for example, $\mathcal{L} = 0.95$) still maintaining the PDR.

For $\mathcal{L} = 2$, Eq. (1) yields $|Z(0)| =$

15 Ohm; therefore $R_B \approx 14$ Ohm should be sufficient to provide DC stability. In this case, the ratio of $\eta_{no_L}/\eta \approx 3.8$ dB. For $\mathcal{L} = 3$, this ratio increases to 5.4 dB. This thought experiment does not consider any variation in the P_{LO}/P_J ratio between the NDR and PRD regimes. Nevertheless, it suggests that the inductorless bias may be a promising approach for achieving a more significant gain enhancement in the NDR regime.

In conclusion, we have demonstrated an increase in conversion gain in the NbN HEB mixer when it is biased in the negative differential resistance (NDR) regime. This biasing approach should reduce the

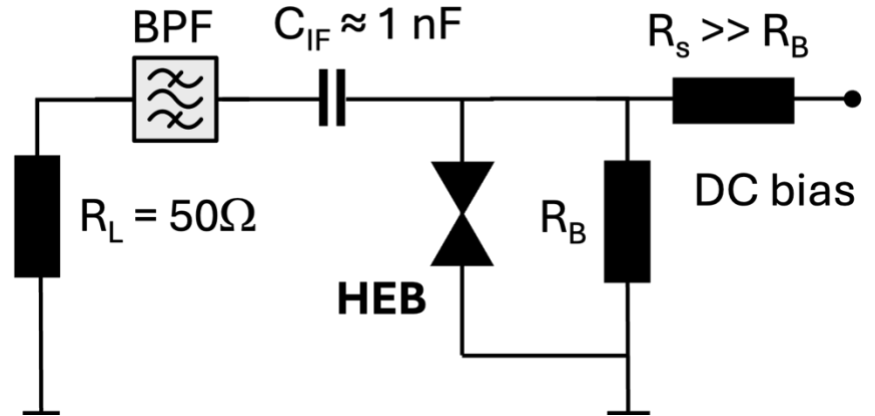


Figure 4. Inductorless bias concept for enabling large values of self-heating parameter \mathcal{L} . Bias resistor R_B is placed close to the HEB device and its value is smaller than $|Z(0)|$ (see Eq. (1)).

contributions of Johnson noise and IF-line noise to the overall system noise temperature. Based on the shape of the IVCs, the value of self-heating parameter \mathcal{L} achieved in Figs. 2 and 3 appears to be moderate, slightly exceeding unity. Larger values of \mathcal{L} can lead to larger conversion values. Future work will test the experimental boundary suggested by Eq. (4) and will explore the feasibility of an inductorless DC-bias configuration, in which only the conditions of Eq. (3a) apply, and a significantly larger overall conversion gain may be attainable. The impact of NDR biasing on the intrinsic HEB noise, and therefore on the system noise temperature, represents the next phase of this research and will be addressed in forthcoming studies.

The research described in this paper was carried out at the Jet Propulsion Laboratory, California Institute of Technology, under a contract with the National Aeronautics and Space Administration. CY acknowledges the support from the NASA Postdoctoral Program.

AUTHOR DECLARATIONS

Conflict of Interest

The authors have no conflicts to disclose.

AUTHOR CONTRIBUTIONS

Chang Yoo: Conceptualization (supporting); formal analysis (equal); methodology (equal); investigation (lead); writing/review and editing (equal). **Akim Babenko:** Conceptualization (supporting); formal analysis (equal); methodology (equal), writing/review and editing (equal), funding acquisition (supporting). **Boris Karasik:** Conceptualization (lead); formal analysis (equal); methodology (equal); funding acquisition (lead), project administration (lead), writing/original draft preparation (lead).

DATA AVAILABILITY

The data that support the findings of this study are available from the corresponding author upon reasonable request.

REFERENCES

1. M. De Lucia, P. Dal Bo, E. Di Giorgi, T. Lari, C. Puglia, and F. Paolucci, *Instruments* **8**, 47 (2024).
2. B. S. Karasik, A. V. Sergeev, and D. E. Prober, *IEEE Trans. Terahertz Sci. Technol.* **1**, 97 (2011).
3. E.M. Gershenzon, G.N. Gol'tsman, I.G. Gogidze, Y.P. Gousev, A.I. Elant'ev, B.S. Karasik, and A.D. Semenov, *Sverkhprovodimost (KIAE)* **3**, 2143 (1990).
4. W. Zhang, W. Miao, Y. Ren, K.-M. Zhou, and S.-C. Shi, *Superconductivity* **2**, 100009 (2022).
5. K. D. Irwin, *Appl. Phys. Lett.* **66**, 1998 (1995).
6. K.D. Irwin and G.C. Hilton, in *Cryogenic particle detection*, edited by Christian Enss (Springer Berlin Heidelberg, Berlin, Heidelberg, 2005), pp. 63.
7. K.D. Irwin, G.C. Hilton, D.A. Wollman, and J.M. Martinis, *J. Appl. Phys.* **83**, 3978 (1998).
8. H. Ekstrom, B. S. Karasik, E. L. Kollberg, and K. S. Yngvesson, *IEEE Trans. Microw. Theory Techn.* **43**, 938 (1995).
9. R. F. Su, Y. D. Zhang, X. C. Tu, X. Q. Jia, C. H. Zhang, L. Kang, B. B. Jin, W. W. Xu, H. B. Wang, J. Chen, and P. H. Wu, *Supercond. Sci. Technol.* **32**, 105002 (2019).
10. Y. Zhuang and K. S. Yngvesson, *12th Int. Symp. Space THz Technol. (ISSTT 2001)*, 131 (2001).
11. Y. Zhuang and K. S. Yngvesson, *13th Int. Symp. Space THz Technol. (ISSTT 2002)*, 463 (2002).
12. Y. Zhuang, D. Gu, and K. S. Yngvesson, *14th Int. Symp. Space THz Technol. (ISSTT 2003)*, 289 (2003).
13. D. Gu, Y. Zhuang, and S. Yngvesson, *15th Int. Symp. Space THz Technol. (ISSTT 2004)*, 218 (2004).
14. A. Trifonov, C. Y. E. Tong, R. Blundell, S. Ryabchun, and G. Gol'tsman, *IEEE Trans. Appl. Supercond.* **25**, 1 (2015).
15. G.T. Munsterman, *APL Technical Digest* **4**, 2 (1965).
16. R. Morariu, J. Wang, A. C. Cornescu, A. Al-Khalidi, A. Ofiare, J. M. L. Figueiredo, and E. Wasige, *IEEE Trans. Microw. Theory Techn.* **67**, 4332 (2019).

17. C. Kidner, I. Mehdi, J. R. East, and G. I. Haddad, *IEEE Trans. Microw. Theory Techn.* **38**, 864 (1990).
18. L. Wang, J. M. L. Figueiredo, C. N. Ironside, and E. Wasige, *IEEE Trans. Electron Dev.* **58**, 343 (2011).
19. M. E. Hines, *Bell Sys. Tech. J.* **39**, 477 (1960).
20. L. I. Smilen and D. C. Youla, *Proc. IRE* **49**, 1206 (1961).
21. B.S. Karasik and A.I. Elantev, *Proc. 6th Int. Symp. Spc. THz Technol.*, 229 (1995).
22. B. S. Karasik and A. I. Elantiev, *Applied Physics Letters* **68**, 853 (1996).
23. A. I. Elant'ev and B. S. Karasik, *Fiz. Nizk. Temp.* **15**, 675 (1989).
24. B. S. Karasik and W. R. Mcgrath, *Int. J. Infrared & Millim. Waves* **20**, 21 (1999).
25. A. Skalare, W. R. McGrath, B. Bumble, and H. G. LeDuc, *IEEE Trans. Appl. Supercond.* **13**, 160 (2003).
26. J. R. Gao, M. Hajenius, Z. Q. Yang, J. J. A. Baselmans, P. Khosropanah, R. Barends, and T. M. Klapwijk, *IEEE Trans. Appl. Supercond.* **17**, 252 (2007).
27. J. R. Gao, J. N. Hovenier, Z. Q. Yang, J. J. A. Baselmans, A. Baryshev, M. Hajenius, T. M. Klapwijk, A. J. L. Adam, T. O. Klaassen, B. S. Williams, S. Kumar, Q. Hu, and J. L. Reno, *Appl. Phys. Lett.* **86** (2005).
28. J. F. Young, B. M. Wood, H. C. Liu, M. Buchanan, D. Landheer, A. J. SpringThorpe, and P. Mandeville, *Appl. Phys. Lett.* **52**, 1398 (1988).
29. H. C. Liu, *Appl. Phys. Lett.* **53**, 485 (1988).
30. D. Wilms Floet, E. Miedema, T. M. Klapwijk, and J. R. Gao, *Appl. Phys. Lett.* **74**, 433 (1999).
31. W. Miao, Y. Delorme, A. Feret, R. Lefevre, B. Lecomte, F. Dauplay, J.-M. Krieg, G. Beaudin, W. Zhang, Y Ren, and S.-C. Shi, *J. Appl. Phys.* **106**, 103909 (2009).
32. A. D. Semenov, R. S. Nebosis, Yu P. Gousev, M. A. Heusinger, and K. F. Renk, *Phys. Rev. B* **52**, 581 (1995).

33. M. Sidorova, A. Semenov, H.-W. Hübers, K. Ilin, M. Siegel, I. Charaev, M. Moshkova, N. Kaurova, G. N. Goltsman, X. Zhang, and A. Schilling, *Phys. Rev. B* **102**, 054501 (2020).